

ESI

Chiral Magnetic Metal-Organic Frameworks of Mn^{II} with Achiral Tetrazolate-Based Ligand by Spontaneous Resolution

Xiao-Lan Tong,^a Tong-Liang Hu,^a Jiong-Peng Zhao,^a Yue-Kui Wang,^b Hui Zhang,^c and Xian-He Bu^{*a}

^a Department of Chemistry, and Tianjin Key Lab on Metal and Molecule-based Material Chemistry, Nankai University, Tianjin 300071, China. E-mail: buxh@nankai.edu.cn. Fax: +86-22-23502458;

^b Institute of Molecular Science, Shanxi University, Taiyuan 030006, China;

^c Department of Chemistry, Xiamen University, Xiamen 363105, China.

Materials and Physical Measurements. All the reagents for synthesis were purchased from commercial sources and used as received. Elemental analyses (C, H, and N) were performed on a Perkin-Elmer 240C analyzer, and IR spectra were measured on a Tensor 27 OPUS (Bruker) FT-IR spectrometer with KBr pellets. The X-ray powder diffraction (XRPD) was recorded on a Rigaku D/Max-2500 diffractometer at 40 kV, 100 mA for a Cu-target tube and a graphite monochromator. Simulation of the XRPD spectra was carried out by the single-crystal data and diffraction-crystal module of the Mercury (Hg) program available free of charge via the Internet at <http://www.iucr.org>. Magnetic data were collected at Nankai University using crushed crystals of the sample on a Quantum Design MPMS XL-7 SQUID magnetometer. The diamagnetic corrections were evaluated from Pascal's constants. The solid-state circular dichroism (CD) spectra were recorded on a Jasco J-715 spectropolarimeter with KCl pellets.

The procedure for getting the CD spectra for the enantiomorphs **1a** and **1b**, is as follows: firstly we chose a large crystal and measured it on the SCX-Mini diffractometer to determine its absolute structure, then we used the same crystal (after removing the glue which used to mount it on a glass fiber for X-ray diffraction measurement) to measure its CD spectra on a Jasco J-715 spectropolarimeter. The same procedures were done repeatedly to find the crystal with another space group, and then measured its CD spectra using the same crystal.

Synthesis of **1 (**1a** and **1b**).** A buffer layer of methanol/water (10 mL, v: v=1:1) was carefully layered over a water solution (3 mL) of MnCl₂·4H₂O (0.1 mmol). Then a solution of HL (0.1 mmol) in methanol (3 mL) was layered on the buffer layer. Pale purple block crystals were obtained after three weeks and washed with water and ethanol and dried in air (ca. 30% yield based on HL). Anal. Calcd for C₁₆H₁₂MnN₁₀O₂: C, 44.56; H, 2.80; N, 32.48. Found: C, 44.28; H, 2.95; N, 32.05. IR (KBr pellet, cm⁻¹): $\tilde{\nu}$ = 3432w, 3227w, 1666s, 1590s, 1568s, 1449m, 1243m, 1019w, 929w, 897m, 826m, 706s, 659m.

X-ray Crystallography. Complexes **1** (**1a** and **1b**) were collected on a computer-controlled on a SCX-Mini diffractometer equipped with a graphite crystal monochromator situated in the incident beam. The determinations of unit cell parameters and data collections were performed with Mo-K α radiation (λ = 0.71073 Å) at 293(2) K and unit cell dimensions were obtained with least-squares refinements. The program SAINT^[1] was used for integration of the diffraction profiles. All the structures were solved by direct methods using the SHELXS program of the SHELXTL package and refined by full-matrix least-squares methods with SHELXL.^[2] Metal atoms in the complexes (**1a** and **1b**) were located from the *E*-maps and other non-hydrogen atoms were located in successive difference Fourier syntheses

and refined with anisotropic thermal parameters on F^2 . The hydrogen atoms of the ligand were generated geometrically; and the hydrogen atoms of the water molecules were located from difference maps and refined with isotropic temperature factors.

- [1] Bruker AXS, SAINT Software Reference Manual, Madison, WI, 1998.
[2] G.M. Sheldrick, SHELXTL NT Version 5.1. Program for Solution and Refinement of Crystal Structures, University of Gottingen, Germany, 1997.

The excited-state crystal wave functions Ψ_r^p corresponding to the ligand excited states ϕ_i^p ($p = 1,2$) for the unit cell.

$$\Psi_{A_1}^p = \frac{1}{\sqrt{8}}(\phi_1^p + \phi_2^p + \phi_3^p + \phi_4^p + \phi_5^p + \phi_6^p + \phi_7^p + \phi_8^p)$$

$$\Psi_{A_2}^p = \frac{1}{\sqrt{8}}(\phi_1^p + \phi_2^p + \phi_3^p + \phi_4^p - \phi_5^p - \phi_6^p - \phi_7^p - \phi_8^p)$$

$$\Psi_{B_1}^p = \frac{1}{\sqrt{8}}(\phi_1^p - \phi_2^p + \phi_3^p - \phi_4^p + \phi_5^p - \phi_6^p + \phi_7^p - \phi_8^p)$$

$$\Psi_{B_2}^p = \frac{1}{\sqrt{8}}(\phi_1^p - \phi_2^p + \phi_3^p - \phi_4^p - \phi_5^p + \phi_6^p - \phi_7^p + \phi_8^p)$$

$$\Psi_{1E_g}^p = \frac{1}{\sqrt{4}}(-\phi_2^p + \phi_4^p + \phi_5^p - \phi_7^p)$$

$$\Psi_{1E_g}^p = \frac{1}{\sqrt{4}}(\phi_1^p - \phi_3^p + \phi_6^p - \phi_8^p)$$

$$\Psi_{2E_g}^p = \frac{1}{\sqrt{4}}(\phi_1^p - \phi_3^p - \phi_6^p + \phi_8^p)$$

$$\Psi_{2E_g}^p = \frac{1}{\sqrt{4}}(\phi_2^p - \phi_4^p + \phi_5^p - \phi_7^p)$$

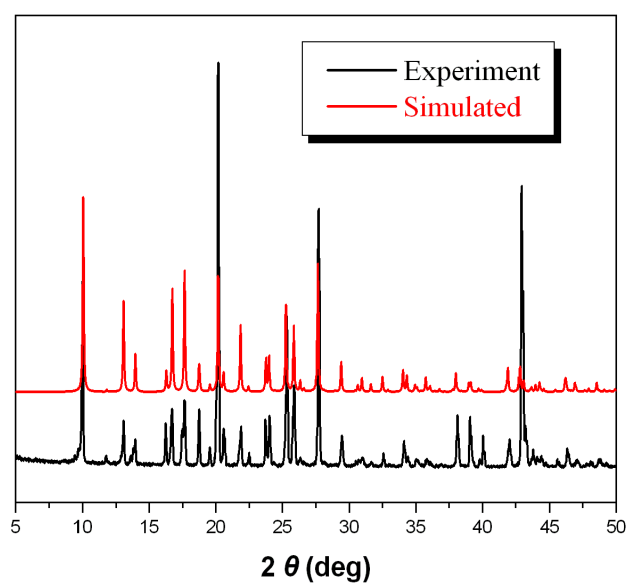


Fig.S1. XRPD patterns for **1**

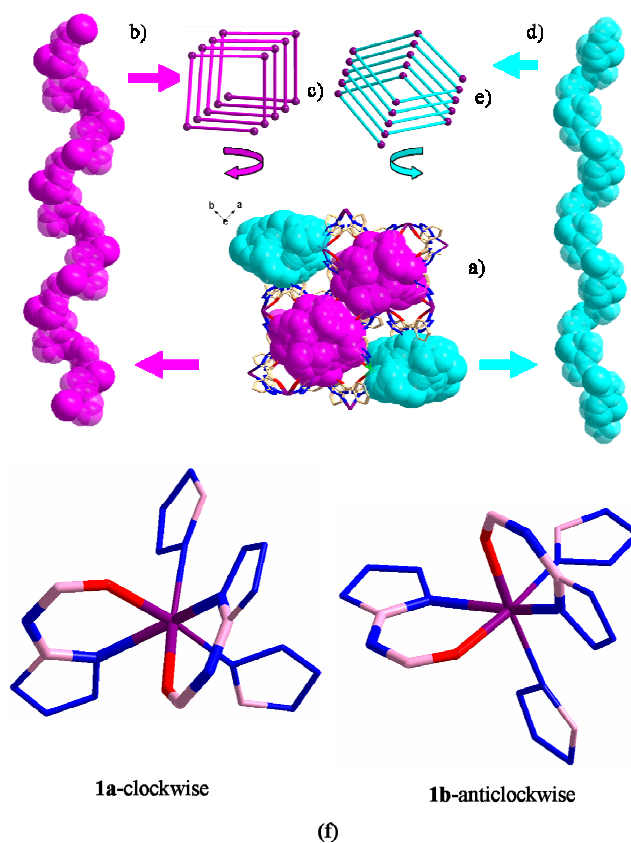


Fig. S2. a) Space-filling views and capped sticks representations of the 3D chiral framework of **1a**. b) Space-filling views of the right-handed helix in **1a**. c) The 4_1 helical axis corresponding to the right-handed helix in **1a**. d) Space-filling views of the left-handed helix in **1a**. e) The 2_1 helical axis corresponding to the left-handed helix in **1a**.

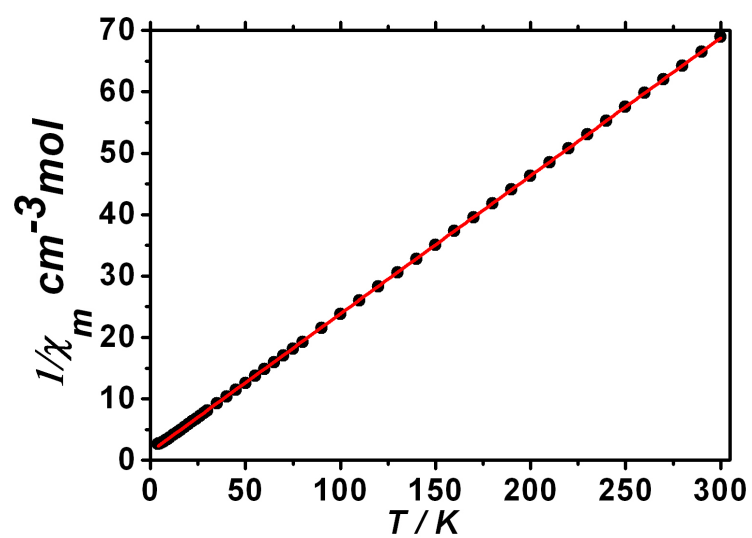


Fig. S3 Curie plot for complex 1. The solid line is the best fit to the Curie-Weiss law..

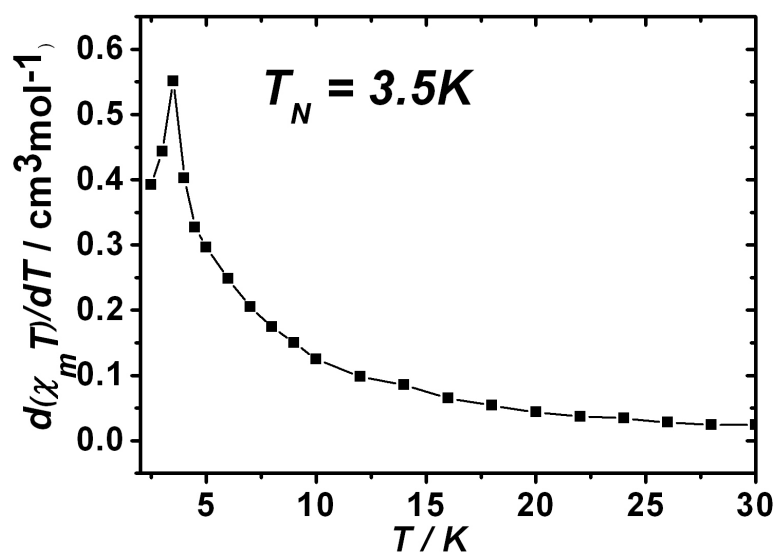


Fig. S4 The $d(\chi_m T)/dT$ vs T derivative curve.

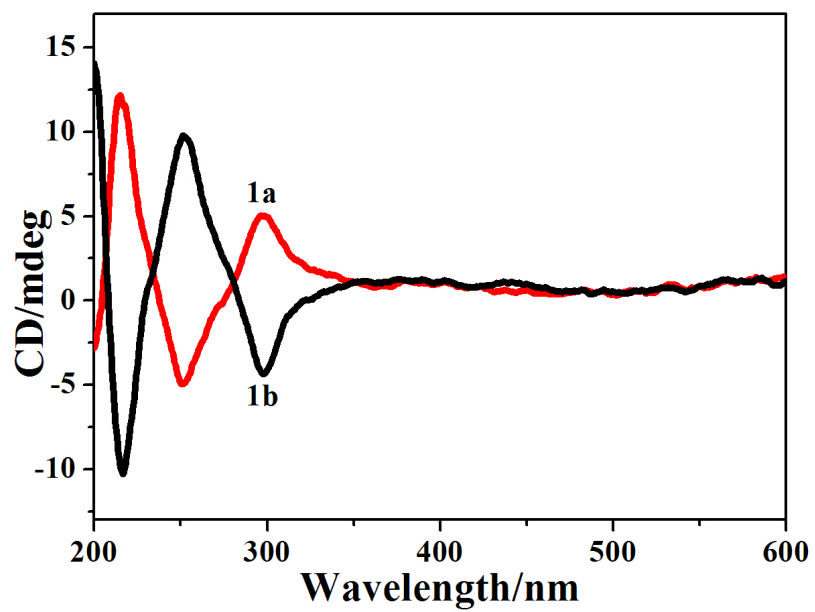


Fig. S5 The solid-state CD spectra for complexes **1a** (red) and **1b** (black).

Table S1. Calculated Excitation Energies, Oscillator and Rotational Strengths.

No	Γ	$\lambda(\text{nm})$	f	$R(\text{DBM})$
1	1^1B_2	266.00	-----	-----
2	1^1E	265.46	0.0693	1.0838
3	1^1B_1	261.53	-----	-----
4	2^1A_1	260.18	-----	-----
5	1^1A_2	259.75	0.2542	-1.2749
6	2^1E	248.40	0.0049	0.1912
7	2^1B_2	205.80	-----	-----
8	3^1E	203.62	0.2088	2.1519